Supporting Information

Contact-free magnetic resonance imaging and spectroscopy with acoustic levitation

Smaragda-Maria Argyri[1a], Leo Svenningsson[1a], Feryal Guerroudj[1], Diana Bernin[1], Lars Evenäs[1]*, and Romain Bordes[1]*

1 Department of Chemistry and Chemical Engineering, Chalmers University of Technology, Gothenburg, Sweden

[a]: Authors contributed equally.

*: Corresponding author.

E-mail address: lars.evenas@chalmers.se

E-mail address: bordes@chalmers.se

Experimental set-up

Mechanical lift

Fig. S1. Photograph of the mechanical lift that was used for the transportation of the demagnetized acoustic levitator with the levitator sample in the MRI-bore.

Frequency response of acoustic levitator

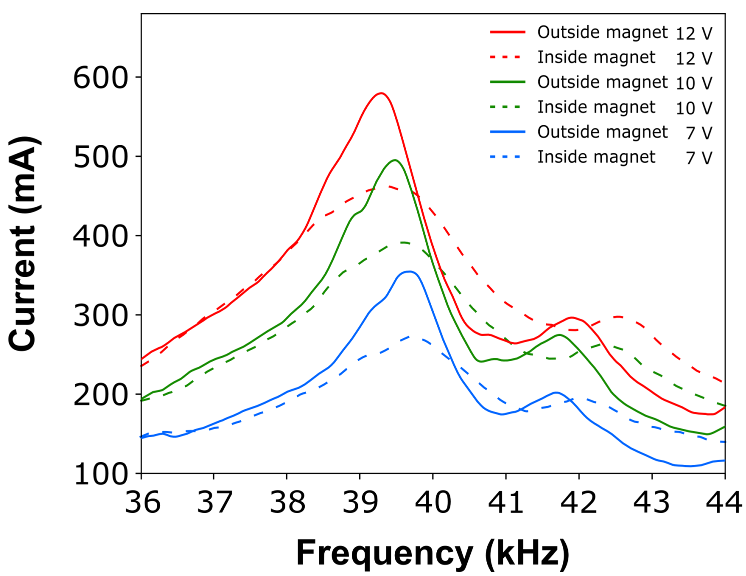

Fig. S2. Frequency response of the demagnetized levitator inside (continuous lines) and outside (dashed lines) the magnet at 7 (lower, blue lines), 10 (middle, green lines), and 12 (upper, red lines) volt.

Magnetic resonance images

Droplet imaging and voxel selection

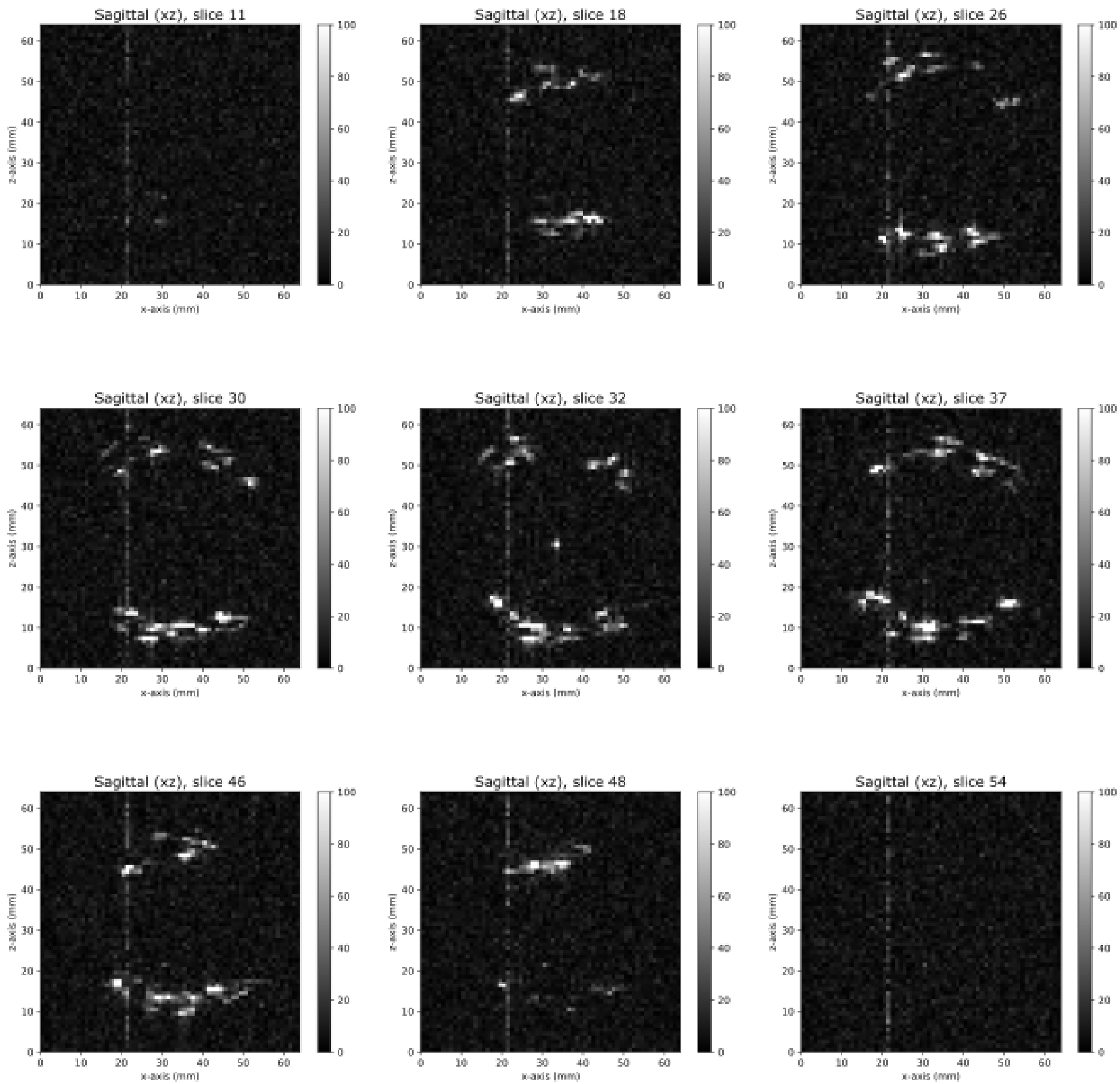

Fig. S3. RARE MR images while a droplet of hexadecane was acoustically levitated at 9.0 V on different 1 mm thick slices along the sagittal (*xz*) plane where the transducers are visible too. We set a field of view 64x64 mm, ROI of 64x64 pixels, 8 averages, repetition time of 3000 ms, echo time of 2.28 ms, bp32 excitation and refocusing pulse, and RARE factor 1. The spherical microliter droplet with a radius of approximately 1 mm is visible only on the central magnetic resonance image (slice 32).

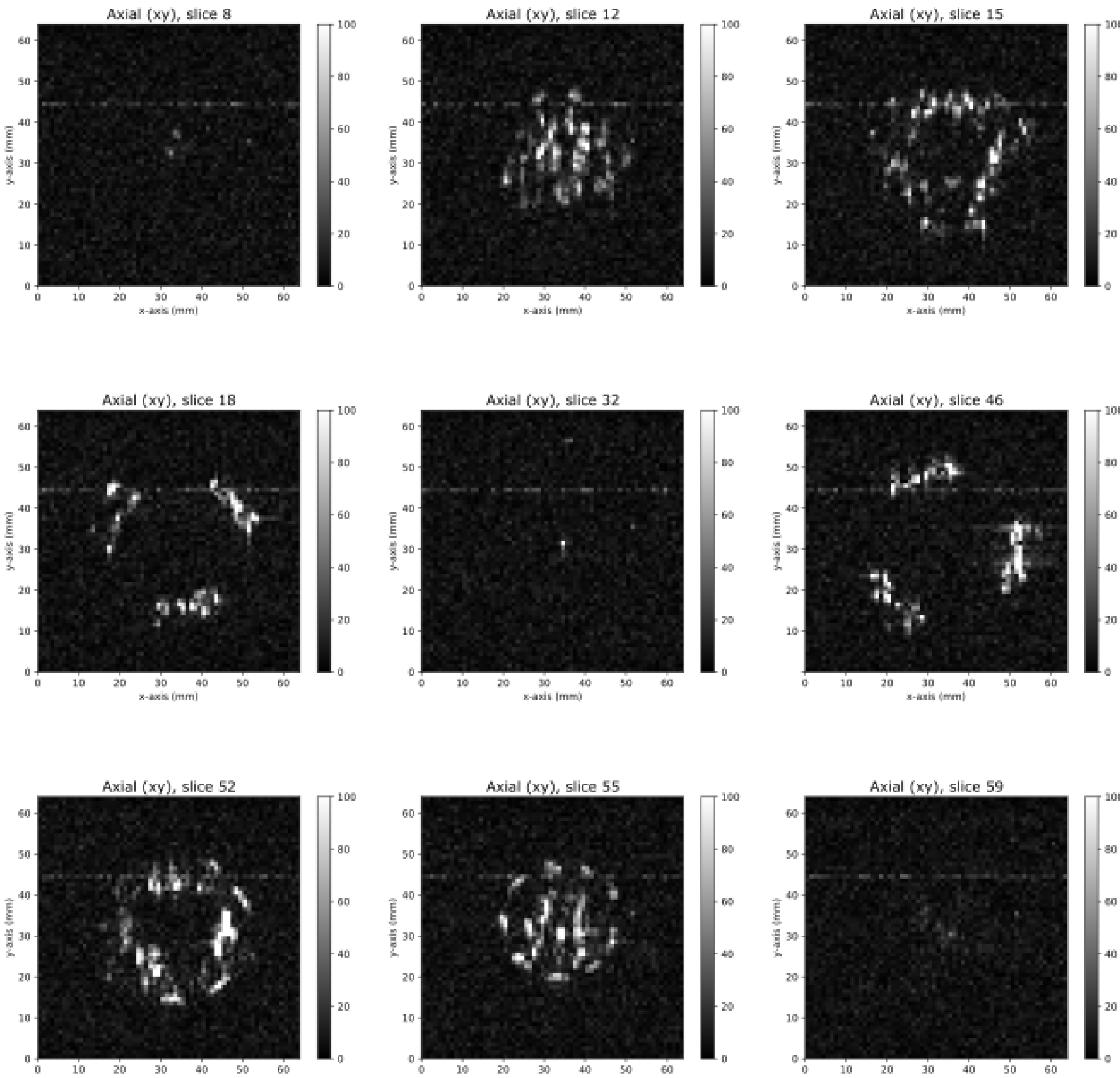

Fig. S4. RARE MR images while a droplet of hexadecane was acoustically levitated at 9.0 V on different 1 mm thick slices along the axial (*xy*) plane where the transducers are visible too. We set a field of view 64x64 mm, ROI of 64x64 pixels, 8 averages, repetition time of 3000 ms, echo time of 2.28 ms, bp32 excitation and refocusing pulse, and RARE factor 1. The spherical microliter droplet with a radius of approximately 1 mm is visible only on the central magnetic resonance image (slice 32).

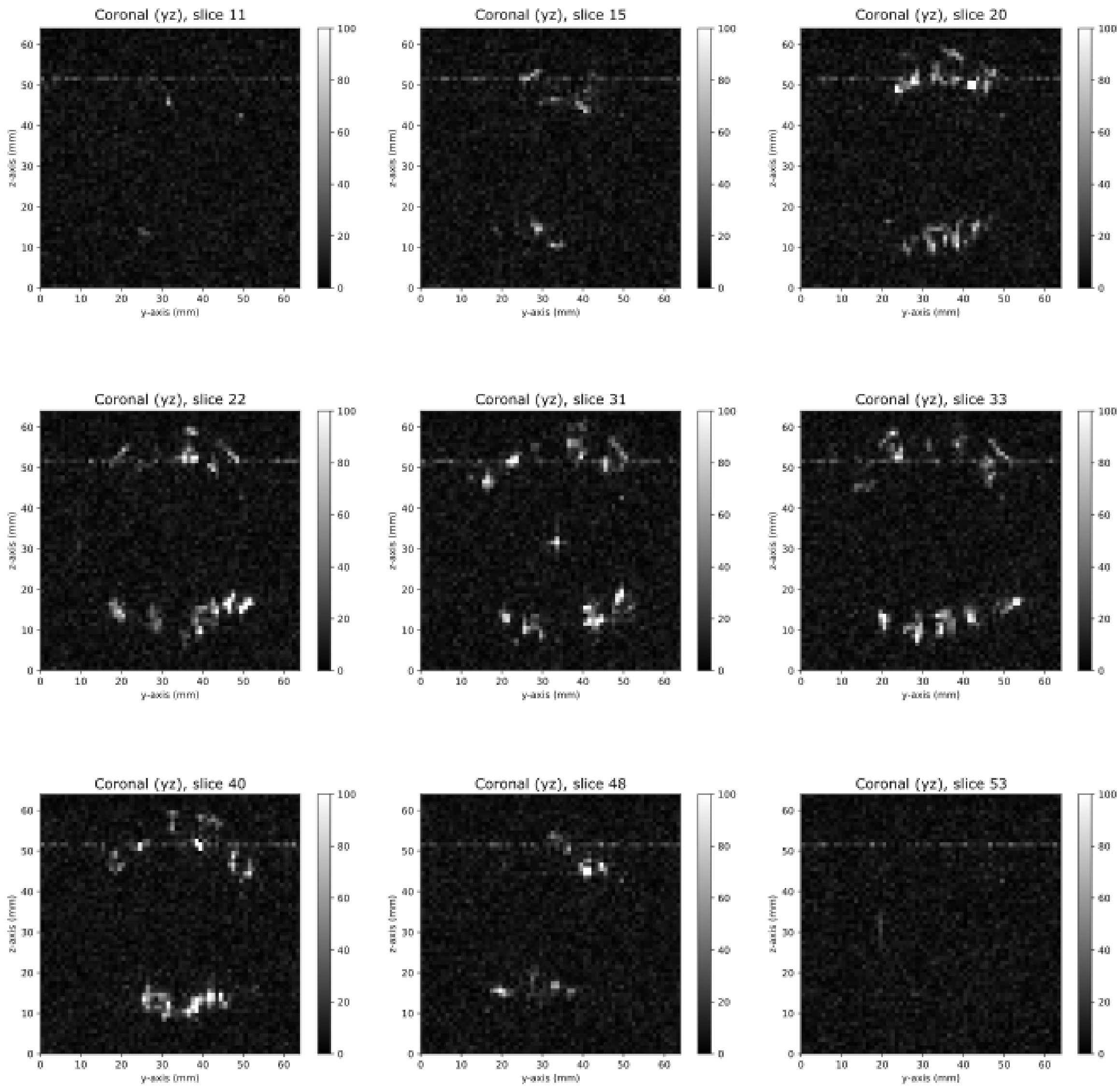

Fig. S5. RARE MR images while a droplet of hexadecane was acoustically levitated at 9.0 V on different 1 mm thick slices along the coronal (*yz*) plane where the transducers are visible too. We set a field of view 64x64 mm, ROI of 64x64 pixels, 8 averages, repetition time of 3000 ms, echo time of 2.28 ms, bp32 excitation and refocusing pulse, and RARE factor 1. The spherical microliter droplet with a radius of approximately 1 mm is visible only on the central magnetic resonance image (slice 31).

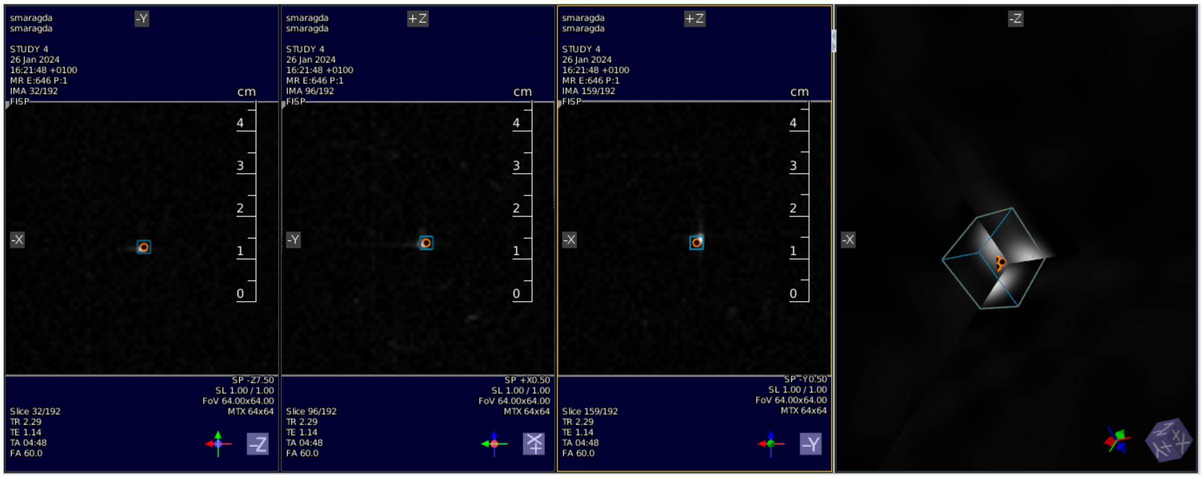

Fig. S6. True-FISP MR images with a 3x3x3 mm voxel selections around an acoustically levitated droplet of canola oil at 9.0 V along the axial (*xy*), sagittal (*xz*) and coronal (*yz*) planes, and 3D intersection of the slices depicting the droplet. We set a field of view 64x64 mm, ROI of 64x64 pixels, 1 average, repetition time of 2.29 ms, echo time of 1.14 ms.

Exploding droplet

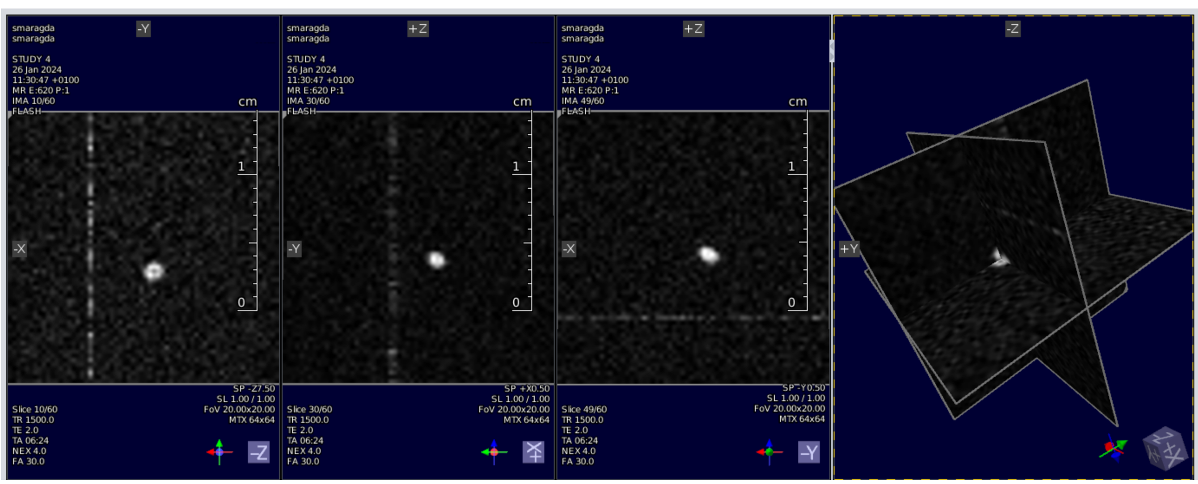

Fig. S7. FLASH MR images of an acoustically levitated droplet of hexadecane at 9.0 V along the axial (*xy*), sagittal (*xz*) and coronal (*yz*) planes, and 3D intersection of the slices depicting the droplet. We set a field of view 20x20 mm, ROI of 64x64 pixels, 4 averages, repetition time of 1500 ms, echo time of 2.0 ms, bp32 excitation pulse.

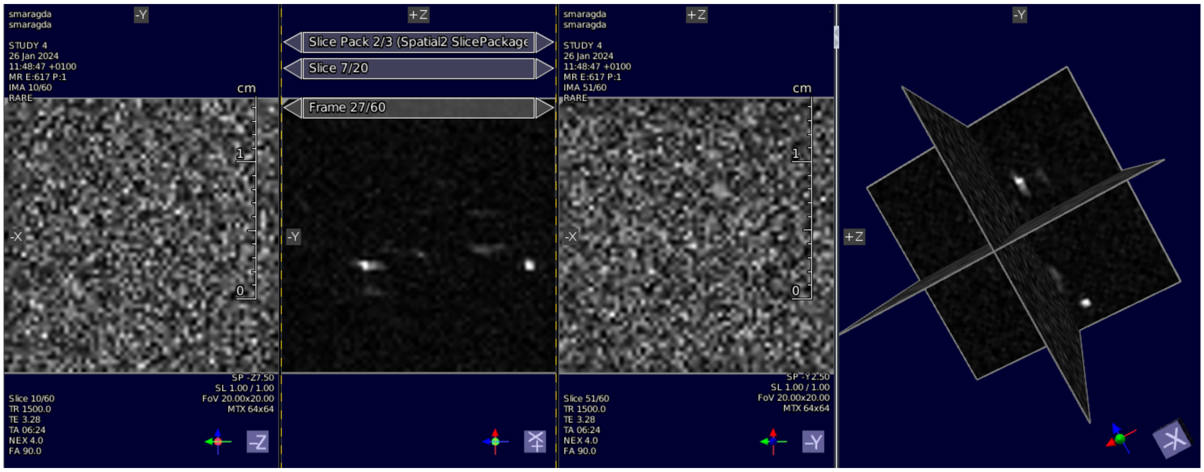

Fig. S8. RARE MR images of the acoustically levitated droplet of hexadecane at 9.0 V that was previously imaged with FLASH in Fig. S7, while being burst along the sagittal (*xz*) plane. No signal was recorded along the axial (*xy*), and coronal (*yz*) planes. In the last subfigure on the right, a 3D intersection of the slices is depicted. We set a field of view 20x20 mm, ROI of 64x64 pixels, 4 averages, repetition time of 1500 ms, echo time of 3.28 ms, calculated excitation, and refocusing function, and RARE factor 1.

FLASH MR images of evaporating water droplet

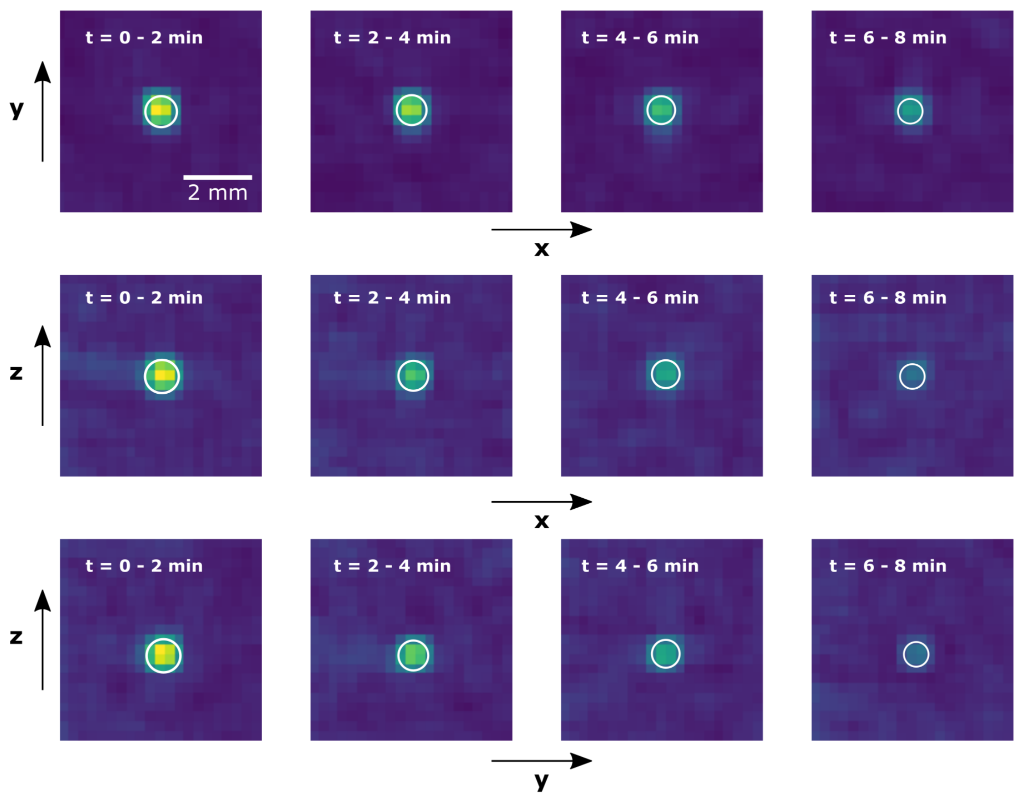

Fig. S9. FLASH MR images of an acoustically levitated droplet of milli-q water, at 10 V, along the axial (*xy*), sagittal (*xz*), and coronal (*yz*) planes, with white overlying fittings of the droplet contours, over a period of approximately 8.5 min. The time in the inset refers to the period of acquisition.

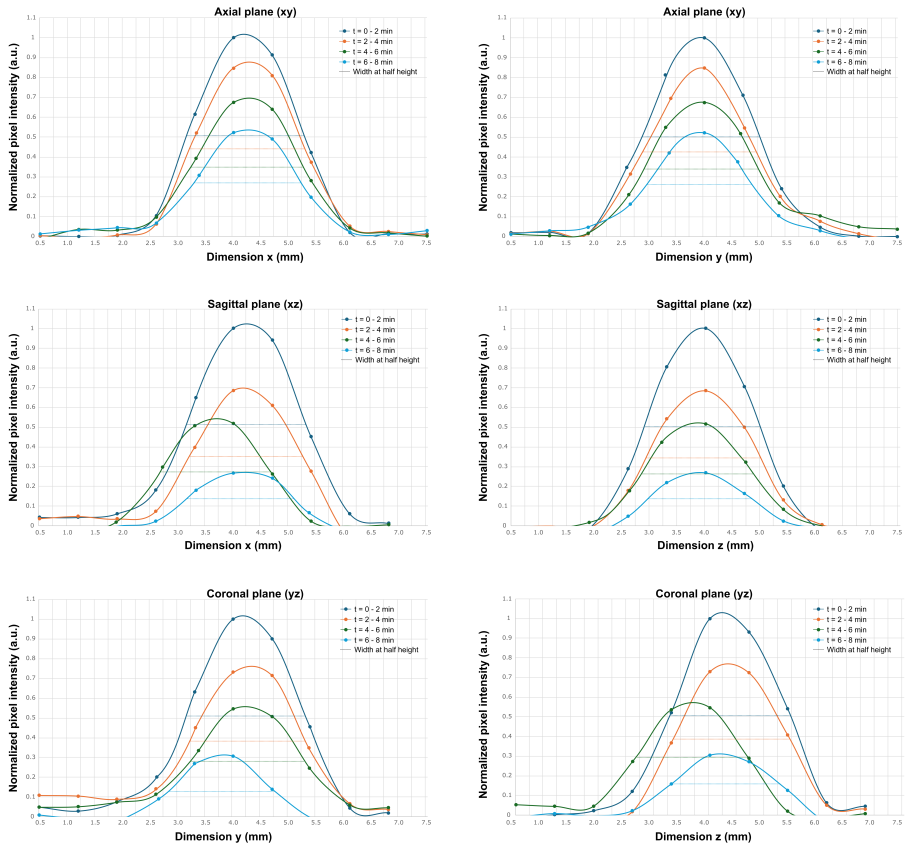

Fig. S10. Normalized pixel intensity around the levitated droplet of water, with respect to the axial distance, from the 4 MR images that were acquired over a period of 8.5 min. The width at half height was estimated, from which we calculated the volume and aspect ratio of the droplet, over time.

The average widths at half the height of the milli-q water droplet are shown in Table S1:

Table S1. Average diameters along the x, y, and z dimension of the water droplet, at each repetition, estimated from the width at half height in Fig. S10.

Dimension (mm)	Repetition 1	Repetition 2	Repetition 3	Repetition 4
x	2.15	2.08	2.03	1.95
y	2.15	2.08	2.08	1.91
z	2.13	2.10	2.05	1.94

From the values shown in Table S1, we calculated the average x, y, and z values, and then determined the volume from the equation:

$$V_{\text{obl}} = \frac{4}{3} \cdot \pi \cdot a \cdot b \cdot c \tag{S1}$$

where, a, b, c are the radii of the droplet along the x, y, and z axial dimensions, respectively.

True-FISP MR images of water evaporation

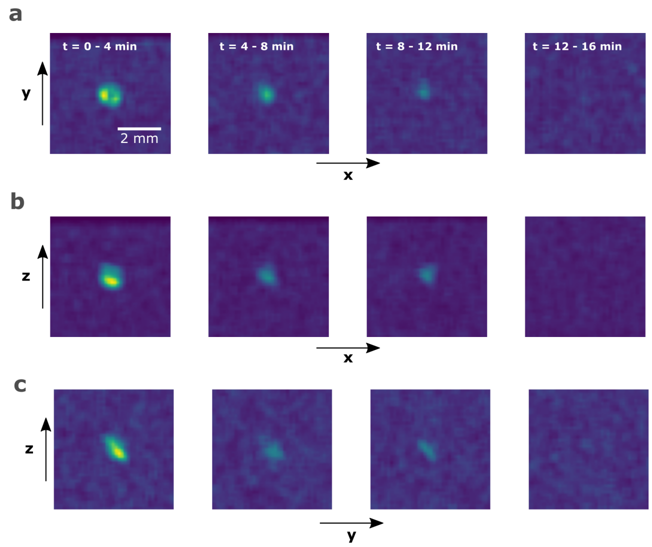

Fig. S11. True-FISP MR images of an acoustically levitated water droplet at 10.0 V along the axial (*xy*), sagittal (*xz*), and coronal (*yz*) planes. We set 32x32 mm field of view, 128x128 pixel ROI, 1 mm slices thickness, 1 average, echo time of 1.783 ms, repetition time of 3.567 ms, 64 segments, 32 slices, bp32 excitation pulse, and applied 4 repetitions with a total acquisition time of 16 min and 25 sec. The images were plotted with Python. The time in the inset refers to the period of acquisition.

True-Fisp MR images of hexadecane at different voltages

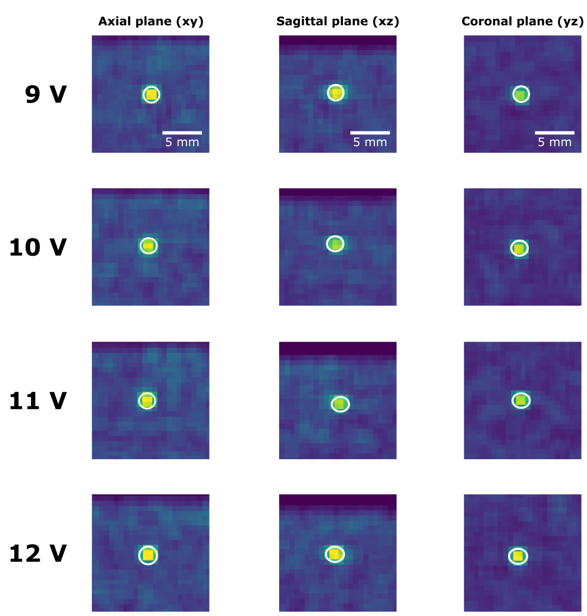

Fig. S12. True-FISP MR images of an acoustically levitated droplet of hexadecane at 9.0 V, 10.0 V, 11.0 V, and 12.0 V, along the axial (*xy*), sagittal (*xz*), and coronal (*yz*) planes, with white overlying fittings of the droplet contours. We set 40x40 mm field of view, 64x64 pixel ROI, 1 mm slices thickness, 1.84 ms for echo time, and 1000 ms for repetition time. The images were plotted with Python and adjusted by applying a 3x3 kernel with values of 0.1.

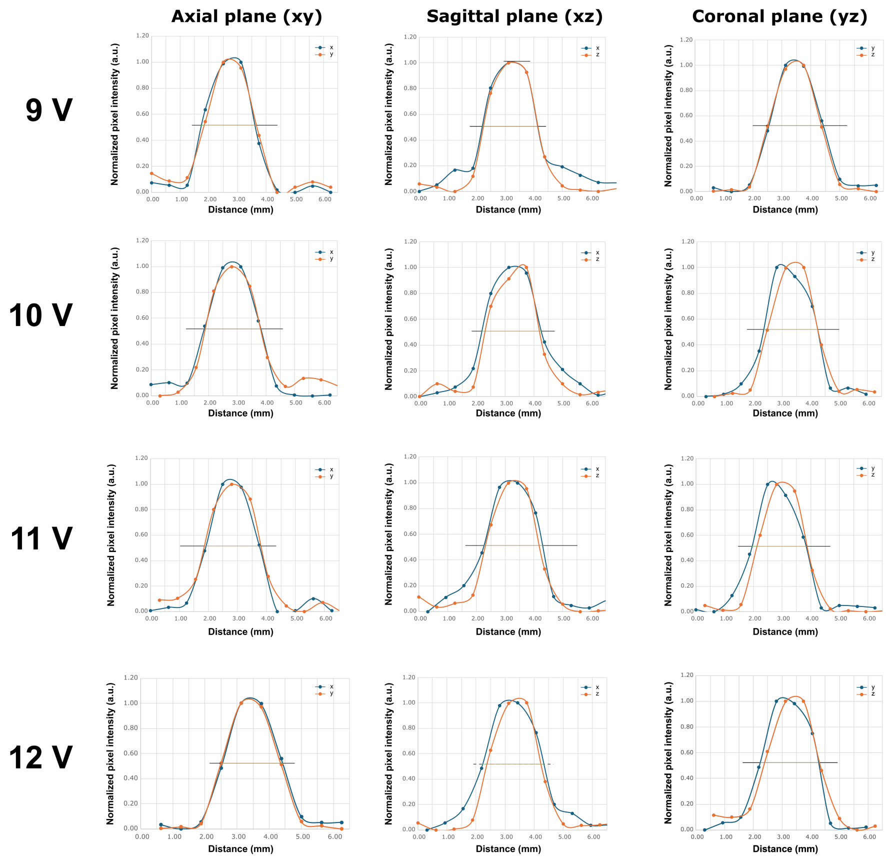

Fig. S13. Normalized pixel intensity around the levitated droplet of hexadecane at different voltages, with respect to the axial distance, along the axial (*xy*), sagittal (*xz*), and coronal (*yz*) planes. The width at half height was determined, from which we calculated the aspect ratio of the droplet.

The average widths at half the height of the hexadecane droplet are shown in Table S2:

Table S2. Average diameters along the x, y, and z dimension of the hexadecane droplet, levitated at different voltages, estimated from the width at half height in Fig. S13.

Voltage (V)	x (mm)	y (mm)	z (mm)
9	1.90	1.85	1.89
10	2.02	1.90	1.83
11	1.95	1.92	1.81
12	2.10	2.06	1.90

From the values presented above and Eq. (S1) we calculated the volume of the droplet to be approximately 3.75 μL.

Nuclear magnetic resonance spectra

Canola oil MR spectra

Table S3. Chemical shifts of signals in ppm, of the MR spectra recorded with the localized pulse sequences STEAM, PRESS, and ISIS, together with the non-localized pulse sequences NSPECT and Single Pulse on an acoustically levitated droplet of canola oil at 9.0 V, in a 7.05 T magnet with a 66 mm diameter MRI probe, compared with the spectrum recorded with a Single Pulse on canola oil in a glass tube, in a 7.05 T magnet with a 5 mm NMR probe.

STEAM (droplet)	PRESS (droplet)	ISIS (droplet)	NSPECT (droplet)	Single Pulse (droplet)	Single Pulse (glass tube)
-	5.53	5.52	5.52	5.53	5.52
-	4.48	4.47	4.47	4.47	4.47
-	4.29	4.30	4.29	4.29	4.29
2.96	2.96	2.98	2.96	2.96	2.97
2.45	2.44	2.44	2.45	2.45	2.45
2.25	2.24	2.23	2.24	2.24	2.23
1.80	1.78	1.79	1.79	1.79	1.79
1.52	1.51	1.51	1.52	1.52	1.51
-	-	-	1.49	1.49	1.49
1.09	1.09	1.10	1.09	1.09	1.10

Table S4. Line widths at half height of signals in Hz, of the MR spectra recorded with the localized pulse sequences STEAM, PRESS, and ISIS, together with the non-localized pulse sequences NSPECT and Single Pulse on an acoustically levitated droplet of canola oil at 9.0 V, in a 7.05 T magnet with a 66 mm diameter MRI probe, compared with the spectrum recorded with a Single Pulse on canola oil in a glass tube, in a 7.05 T magnet with a 5 mm NMR probe.

STEAM (droplet)	PRESS (droplet)	ISIS (droplet)	NSPECT (droplet)	Single Pulse (droplet)	Single Pulse (glass tube)
-	15.63	12.67	10.9	5.55	12.45
-	19.78	13.75	4.48	7.20	6.65
-	16.37	15.24	4.48	5.92	6.04
20.55	14.31	16.53	6.31	6.28	12.60
29.35	8.47	9.74	5.76	5.73	6.96
22.38	23.29	20.38	7.23	7.02	13.97
19.81	21.27	18.73	20.62	18.06	20.84
40.66	7.76	20.88	14.16	14.34	14.71
-	-	-	8.98	9.00	8.14
11.38	10.27	11.02	5.95	5.73	6.50

Series of hexadecane ISIS MR spectra

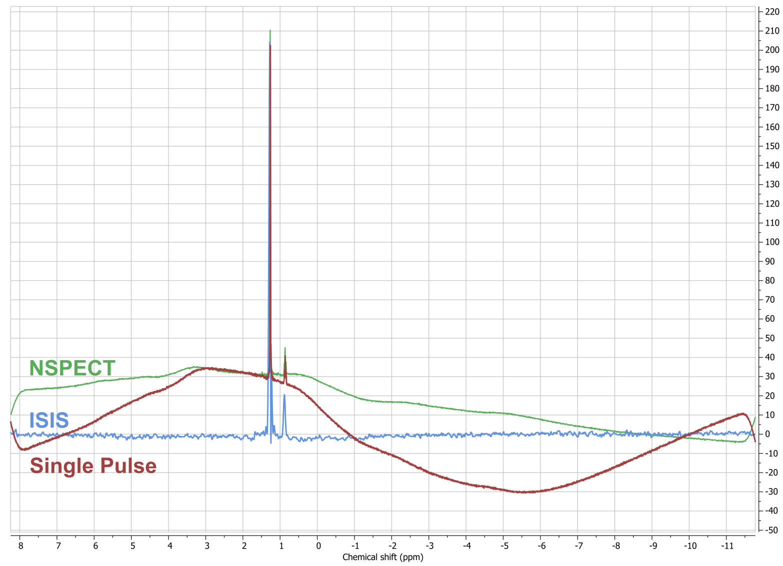

Fig. S14. Baseline comparison between NSPECT (green), ISIS (blue), and Single Pulse (red) of an acoustically levitated hexadecane droplet at 9.0 V. For the pulse sequence ISIS we applied 8 averages (64 ISIS averages), 1500 ms repetition time, on a 3x3x3 mm voxel. For NSPECT and Single Pulse, we applied 40 and 20 averages, respectively, and 1500 ms repetition time. The phase of the spectrum collected with ISIS was manually corrected, and no further adjustments were made.

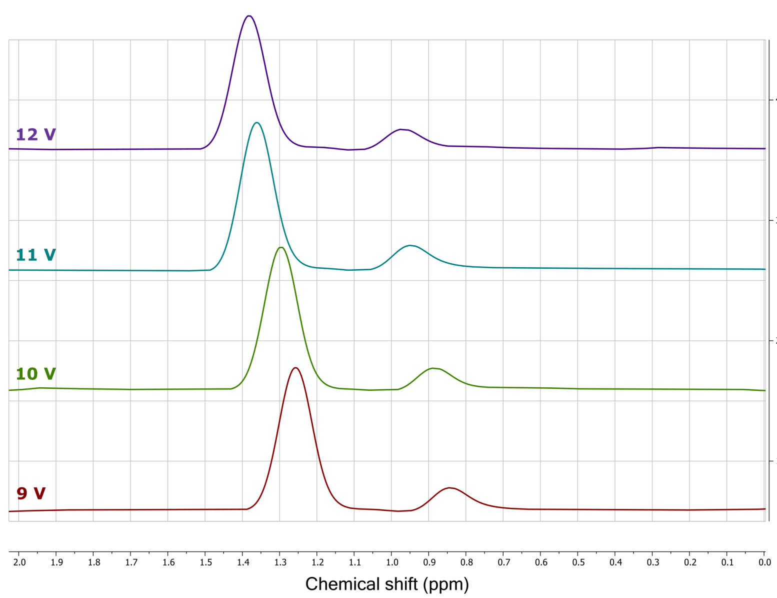

Fig. S15. ISIS MR spectra of an acoustically levitated hexadecane droplet at 9.0 V, 10.0 V, 11.0 V, and 12.0 V. We applied 8 averages (64 ISIS averages), 1500 ms repetition time, on a 3x3x3 mm voxel. We applied 5 Hz exponential line broadening, the phase was manually corrected, and the baselines were corrected by applying Bernstein polynomial fit with an order of 3.

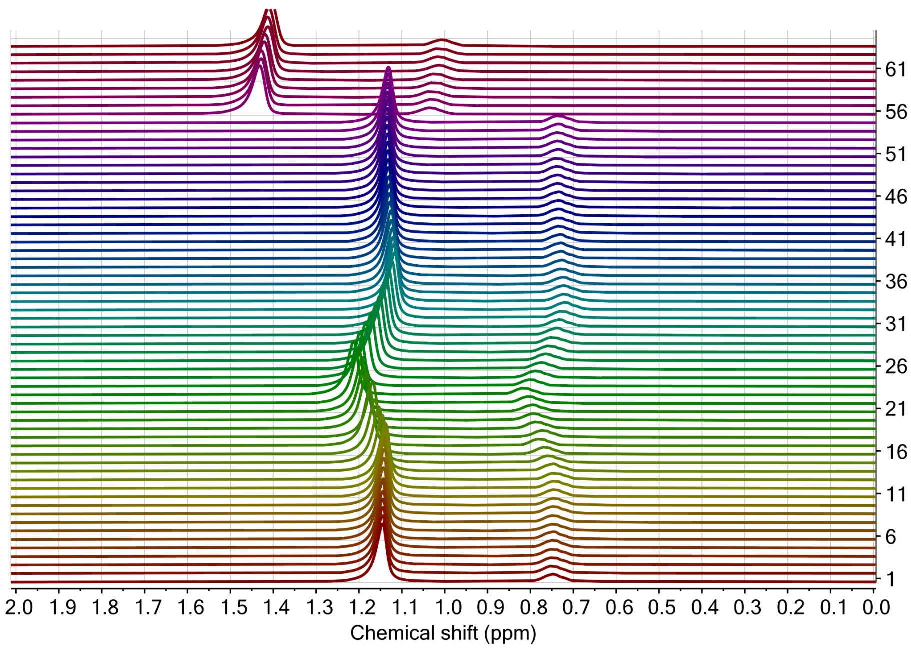

Fig. S16. Series of ISIS MR spectra of an acoustically levitated hexadecane droplet with (from bottom to top) 15 spectra at 9.0 V, 10 spectra with a voltage increase from 9.0 V to 10.0 V with a step of 0.1 V, 10 spectra with a voltage decrease from 10.0 V to 9.0 V with a step of 0.1 V, 20 spectra at 9.0 V, and 7 spectra at 12.0 V. The spectra were acquired by setting 8 averages (64 ISIS averages), 1500 ms repetition time, on a 3x3x3 mm voxel. We applied 5 Hz exponential line broadening, the phase was manually corrected, and the baselines were corrected by applying Bernstein polynomial fit with an order of 3.

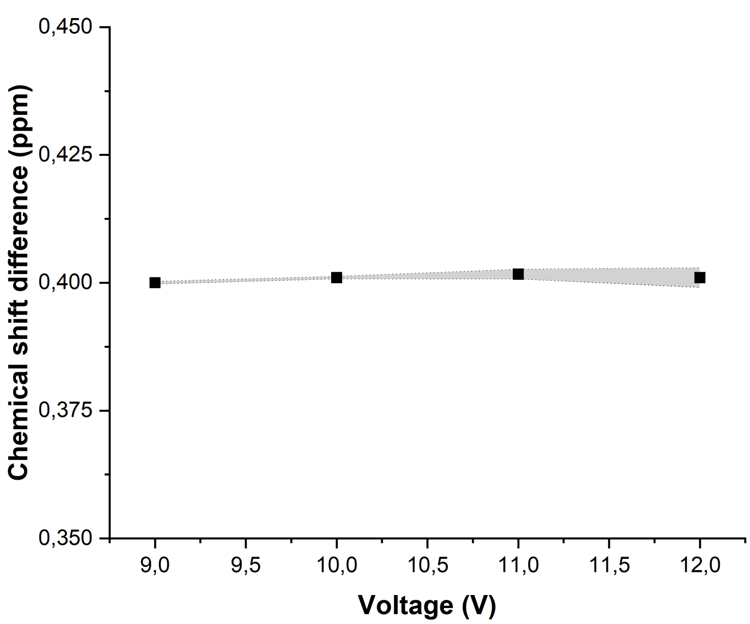

Fig. S17. Chemical shift differences between the signals of hexadecane with respect to the applied voltage. The increased error with voltage is most likely related to a steady-state heating dependence from the pulses. The measurements were repeated a minimum of 3 times and the error was calculated from the standard deviation.

Evaporation of a 50 wt% aqueous TEG droplet

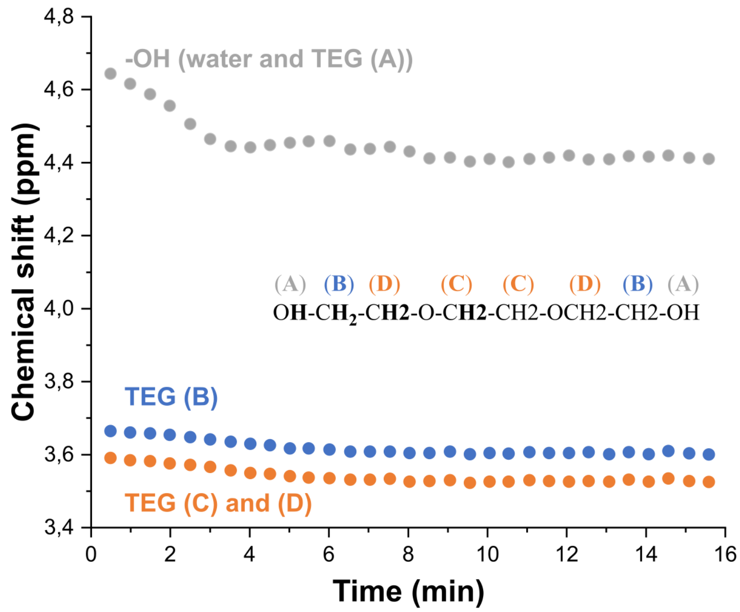

Fig. S18. Chemical shifts of signals present in the 50 wt% TEG solution of the acoustically levitated droplet over time.